frontiers in Materials

ORIGINAL RESEARCH
published: 02 July 2018
doi: 10.3389/fmats.2018.00029

Facile MoS_2 Growth on Reduced Graphene-Oxide via Liquid Phase Method

Vasileios Tzitzios[1], Konstantinos Dimos[2,3], Saeed M. Alhassan[1]*, Rohan Mishra[4,5,6], Antonios Kouloumpis[2], Dimitrios Gournis[2], Nikolaos Boukos[7], Manuel A. Roldan[8,9], Juan-Carlos Idrobo[8], Michael A. Karakassides[2], Georgia Basina[1], Yasser Alwahedi[1], Hae Jin Kim[10], Marios S. Katsiotis[1,11], Michael Fardis[4], Albina Borisevich[5], Stephen J. Pennycook[12], Sokrates T. Pantelides[4,5] and George Papavassiliou[7]**

[1] Department of Chemical Engineering, Petroleum Institute, Khalifa University of Science and Technology, Abu Dhabi, United Arab Emirates, [2] Department of Materials Science and Engineering, University of Ioannina, Ioannina, Greece, [3] Cambridge Graphene Centre, University of Cambridge, Cambridge, United Kingdom, [4] Department of Physics and Astronomy, Vanderbilt University, Nashville, TN, United States, [5] Materials Science and Technology Division, Oak Ridge National Laboratory, Oak Ridge, TN, United States, [6] Department of Mechanical Engineering and Materials Science, Washington University in St. Louis, St. Louis, MO, United States, [7] Institute of Nanoscience and Nanotechnology, National Centre of Scientific Research Demokritos, Athens, Greece, [8] Center for Nanophase Materials Sciences, Oak Ridge National Laboratory, Oak Ridge, TN, United States, [9] Eyring Materials Center, Arizona State University, Tempe, AZ, United States, [10] Center for Electron Microscopic Research, Korea Basic Science Institute, Daejeon, South Korea, [11] TITAN Cement Company S.A, Attica, Greece, [12] Department of Materials Science and Engineering, National University of Singapore, Singapore, Singapore

OPEN ACCESS

Edited by:
*Wee-Jun Ong, Institute of Materials Research and Engineering (A*STAR), Singapore*

Reviewed by:
Jialiang Wang, University of Wisconsin-Madison, United States
Kazuma Gotoh, Okayama University, Japan

***Correspondence:**
Vasileios Tzitzios
vatzitzios@pi.ac.ae
Saeed M. Alhassan
salhassan@pi.ac.ae
George Papavassiliou
g.papavassiliou@inn.demokritos.gr

Specialty section:
This article was submitted to Carbon-Based Materials, a section of the journal Frontiers in Materials

Received: *09 February 2018*
Accepted: *24 April 2018*
Published: *02 July 2018*

Citation:
Tzitzios V, Dimos K, Alhassan SM, Mishra R, Kouloumpis A, Gournis D, Boukos N, Roldan MA, Idrobo J-C, Karakassides MA, Basina G, Alwahedi Y, Jin Kim H, Katsiotis MS, Fardis M, Borisevich A, Pennycook SJ, Pantelides ST and Papavassiliou G (2018) Facile MoS_2 Growth on Reduced Graphene-Oxide via Liquid Phase Method. Front. Mater. 5:29. doi: 10.3389/fmats.2018.00029

Single and few-layers MoS_2 were uniformly grown on the surface of chemically reduced graphene oxide (r-GO), via a facile liquid phase approach. The method is based on a simple functionalization of r-GO with oleyl amine which seems to affect significantly the MoS_2 way of growth. Scanning-transmission-electron microscopy (STEM) analysis revealed the presence of single-layer MoS_2 on the surface of a few-layers r-GO. This result was also confirmed by atomic-force microscopy (AFM) images. X-ray photoemission spectroscopy (XPS) and Raman spectroscopy were used for in-depth structural characterization. Furthermore, we have successfully applied the method to synthesize MoS_2 nanocomposites with multi wall carbon nanotubes (CN) and carbon nanofibers (CNF). The results demonstrate clearly the selective MoS_2 growth on both carbon-based supports.

Keywords: reduced graphene oxide, MoS_2, hybrid, layered materials, colloidal solutions, chemical synthesis

INTRODUCTION

Due to their unique electronic properties, atomically-thin two-dimensional (2D) materials such as graphene (Geim and Novoselov, 2007), hexagonal boron nitride (h-BN) (Dean et al., 2010) and transition-metal dichalcogenide (Radisavljevic et al., 2011; Lembke and Kis, 2012; Wang et al., 2012) have been attracting increasing attention. Molybdenum disulfide (MoS_2) is a layered 2D material that is traditionally used as a solid-state lubricant and is the major industrial catalyst for the hydrodesulfurization process (HDS) (Li et al., 2011; Kong et al., 2013). Recently, MoS_2 and hybrid MoS_2 materials have been extensively studied as catalysts in the hydrogen evolution reaction (HER) (Liao et al., 2013; Wang et al., 2014; Zheng et al., 2014). In recent years, ultrathin graphene and

MoS_2 crystals have been obtained by either physical or chemical exfoliation methods (Coleman et al., 2011), while large-scale uniform layers have been grown by chemical-vapor-deposition (CVD) techniques (Chen et al., 2016; Samad et al., 2016; Zobel et al., 2016). Both graphene and MoS_2 in monolayer form exhibit unique optical and electrical properties compared with the respective multilayer analogs. MoS_2, which is referred to in the literature as the inorganic analog of graphene, is a semiconductor with a large direct band gap (Conley et al., 2013). The presence of a band gap in monolayer MoS_2 opens new possibilities in electronic, and photonic applications. Furthermore, the edges of MoS_2 monolayers are catalytically active so that increasing the number of such sites is critical for the design of advanced catalysts (Jaramillo et al., 2007).

During the last few years, there has been substantial interest in the literature concerning the synthesis of hybrid materials based on graphene and MoS_2. Kun Chang and Weixiang Chen reported the synthesis of single-layer MoS_2/graphene dispersed in amorphous carbon and tested its electrochemical performance for lithium batteries (Chang and Chen, 2011). The reaction takes place in water under autoclave conditions at 240°C for 24 h. Molybdenum and sulfur precursors $Na_2MoO_4 \bullet 2H_2O$ and sulfocarbamide (NH_2CSNH_2) were used and the final material was annealed at 800°C for 2 h in a H_2/N_2 atmosphere. Ma et al. reported the synthesis of few-layer MoS_2-graphene composites via a cationic surfactant-assisted hydrothermal method followed by a post-annealing step and showed that the electrochemical performance for lithium storage is greatly improved compared to bare MoS_2 (Ma et al., 2014). Following a similar experimental procedure in a two-step hydrothermal synthesis, Quanjun Xiang et al. reported the decoration of MoS_2/graphene heterostuctures with TiO_2 nanoparticles and tested them as non-precious metals photocatalysts for H_2 production (Xiang et al., 2012). In a one-step hydrothermal method, MoS_2/reduced GO was prepared by $(NH_4)_2MoS_4$ reduction in *N,N*'-dimethylformamide (DMF) at 200°C by hydrazine. A transmission-electron-microscopy (TEM) study showed that most of the MoS_2 lies flat on the reduced GO sheets, with some possessing-induced folded edges exhibiting parallel lines (Li et al., 2011).

Summarizing the literature concerning the synthesis of MoS_2/graphene composite nanomaterials via liquid phase reactions, most of the methodologies involve a hydrothermal process for at least 12 h in the 200–240°C temperature range in one- or two-step procedures. Here we report the synthesis of MoS_2/r-GO following a liquid-phase approach. The method is based on the thermolytic decomposition of $(NH_4)_2MoS_4$ by oleyl amine at 350°C in the presence of chemically-exfoliated reduced graphene oxide (r-GO). The presence of exfoliated r-GO nanosheets in the reaction mixture is crucial, providing a confinement environment for the nucleation and growth of the MoS_2. It is shown that r-GO is predominantly decorated by single-layer MoS_2 that lies flat on the r-GO sheets. The MoS_2/RGO composites are surface functionalized efficiently by oleyl amine molecules, making the material dispersible in non-polar solvents such as toluene and hexane.

EXPERIMENTAL SECTION

Materials

Ammonium tetrathiomolybdate ($(NH_4)_2MoS_4$, 99.97%), oleyl amine (90% C-18 content), carbon nanotubes, carbon nanofibers, absolute ethanol and n-hexane were purchased from Sigma-Aldrich and used without any further purification. Graphene oxide was synthesized using a modified Staudenmaier's method (Staudenmaier, 1898; Gengler et al., 2010; Stergiou et al., 2010). Briefly powdered graphite (purum, powder $\leq$0.2 mm, Fluka) were treated by a 2/1 mixture of concentrated H_2SO_4 (Riedelde Haën) and HNO_3 acid, while cooling in an ice–water bath. Subsequently powdered $KClO_3$ (Fluka) were added to the mixture in small portions under vigorous stirring while cooling in an ice-water bath. The reaction was quenched after 18 h by pouring the mixture into ultrapure water. The oxidation product was washed until the pH reached 6.0, and finally dried at room temperature.

Synthesis of MoS_2/Reduced Graphene Oxide

The reduction and functionalization of GO was carried out via a chemical approach. The pristine GO was exfoliated in oleyl amine via probe sonication at room temperature. Subsequently the mixture was heated up to 300°C under H_2-Ar reducing atmosphere for 1 h. The oleyl amine functionalized r-GO was separated by centrifuging at 12,000 rpm, washed twice in ethanol in order to remove the excess of oleyl amine, and finally dried at room temperature.

MoS_2/r-GO nanocomposites were prepared according to the following procedure. Oleyl-amine-functionalized r-GO (40 mg) was dispersed in 10 ml oleyl amine under probe sonication in an inert atmosphere for 15 min. The mixture was then transferred to a heating plate and 20 mg of $(NH_4)_2MoS_4$ was dissolved into the mixture under vigorous magnetic stirring. In the beginning, the temperature was raised to 120°C and kept there for 15 min under a high-purity N_2 blanket. The reaction finally took place at 350°C for 1 h. After cooling the mixture to room temperature, the composite material was precipitated by adding absolute ethanol and was separated by centrifugation (8,000 RPM, 25 min). The washing/separation procedure was repeated until the complete removal of excess oleyl amine molecules and unreacted components. Finally the composite material was dispersed and stored in toluene.

Characterization

The morphology of the composite MoS_2/RGO material was studied by a Nion Ultra STEM 100 aberration-corrected scanning transmission electron microscope (STEM), which is equipped with a Gatan Enfinium spectrometer for Electron Energy Loss Spectroscopy (EELS). The STEM was operated at 60 kV. Additionally, the material was characterized by atomic-force microscopy (AFM), Raman, and X-ray photoelectron spectroscopy (XPS).

XPS measurements were performed under ultrahigh vacuum conditions at a base pressure of 5×10^{-10} mbar in a SPECS GmbH instrument equipped with a monochromatic MgKα

source ($h\nu$ = 1253.6 eV) and a Phoibos-100 hemispherical analyzer. Pulverized samples were dispersed in toluene (1 wt%), and after short sonication and stirring, a minute quantity of the suspensions were drop-cast on evaporated gold films supported on mica substrates and left to dry in air before transferring them to ultrahigh vacuum. The energy resolution was set to 0.3 eV and the photoelectron take-off angle was 45° with respect to the surface normal. Recorded spectra were the average of three scans with energy step set to 0.05 eV and dwell time 1 s. All binding energies were referenced to the Si 2*p* level at 99.15 eV. Spectral analysis included a Shirley background subtraction and peak deconvolution employing mixed Gaussian–Lorentzian functions, in a least squares curve-fitting program (WinSpec) developed at the Laboratoire Interdisciplinaire de Spectroscopie Electronique, University of Namur, Belgium.

Raman spectra were recorded with a micro-Raman (μ-Raman) Renishaw RM1000 system using a laser diode excitation line at 532 nm in the frequency range of 200–2,000 cm^{-1}. Raman scatter was collected by means of an Olympus optical microscope, equipped with 50× and 100× lenses. Using the 50× lens, the probing spot was about 2 μm in diameter, while the laser was operated at 5 mW unless photodecomposition occurred when the power was decreased. The spectrometer was calibrated by recording the spectrum from a Si sample with characteristic Raman peak at 520.7 cm^{-1}. Raman spectra were obtained from samples in the form of drop casted films onto glass substrates. The reported spectra are an average of 3–5 scans.

AFM images were obtained in tapping mode with a 3D Multimode Nanoscope, using Tap-300G silicon cantilevers with a tip radius <10 nm and a force constant of ≈20–75 N m^{-1}. Samples were deposited onto silicon wafers (P/Bor, single side polished) from dilute dispersions of MoS_2/r-GO in toluene by drop casting.

RESULTS AND DISCUSSION

The synthetic procedure for the decoration of r-GO with MoS_2 is illustrated in **Scheme 1**. Oleyl-amine-functionalized exfoliated r-GO sheets were dispersed in oleyl amine, providing nucleation centers for the growth of MoS_2. Then, the thermolytic decomposition of $(NH_4)_2MoS_4$ at 350°C resulted in the formation of a single layer of MoS_2 on the surface of the r-GO. The XRD patterns of MoS_2/r-GO nanocomposite are presented in Figure S1, in the Supplementary Material section. Because of the nanosize regime of the material, the diffraction peaks are quite broad, but it is possible to distinguish four diffraction peaks. The intense broad peak around $2\theta = 24°$ corresponds to the (002) diffraction plane of r-GO, while the other peaks can be assigned to the (101), (103), and (110) lattice planes of MoS_2.

The morphology of the MoS_2/r-GO nanocomposite was examined by atomic- resolution Scanning Transmission Electron Microscopy (STEM) measurements. In **Figure 1**, we present Z-contrast images of the MoS_2 nanosheets on the few-layer r-GO. It is obvious that the MoS_2 layers grow discontinuously on the surface of the r-GO sheets, covering most of their surface by a single- to few-layer MoS_2 films. Furthermore, the images confirm the few-layer nature of the r-GO as well as the presence of isolated single atoms, most likely Mo atoms, and Mo vacancies. The STEM observations indicate very clearly that the oleyl-amine-functionalized r-GO sheets could be an excellent substrate for the nucleation and growth of MoS_2. This effect can be attributed to the presence of oxygen-containing functional groups on the surface of the r-GO or on the weak van der Waals forces (Shi et al., 2012) between the two layered materials, which accommodate the relatively large lattice mismatch between MoS_2 and graphene (∼28%) (Ma et al., 2011).

In order to clarify the role of the r-GO surface functionalization on the growth of the MoS_2 sheets, the synthesis was also done following a similar methodology using GO as staring material, without any previous reduction and surface functionalization. The TEM images, presented in the Supplementary Material section (Figure S2), clearly show that mainly isolated MoS_2 nanosheets grow on the GO surface, but they do not lie flat on the GO sheets. Furthermore, the formation of nanoparticles instead of nanosheets can be observed. This morphology is quite similar with a previously reported work in which the MoS_2/r-GO composites synthesized by mixing GO with $(NH_4)_2MoS_4$ in an alcohol/water medium followed by the $(NH_4)_2MoS_4$ decomposition by HCl acid addition (Koroteev et al., 2011). The above findings prove indirectly that the surface chemistry of the carbon material plays a very important role in the growth of MoS_2. The oxygen-containing functional groups, as already reported, affect the nucleation and growth of the MoS_2 nanosheets, but on the other hand probably suppress the van der Waals forces that are responsible for the flat MoS_2 growth. Finally, STEM-EELS mapping of sulfur and carbon (**Figure 2b**, which corresponds to the white square area of **Figure 2a**) shows

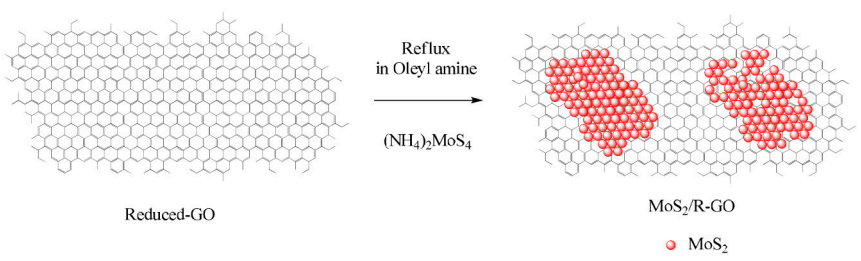

SCHEME 1 | Schematic diagram of the synthetic procedure.

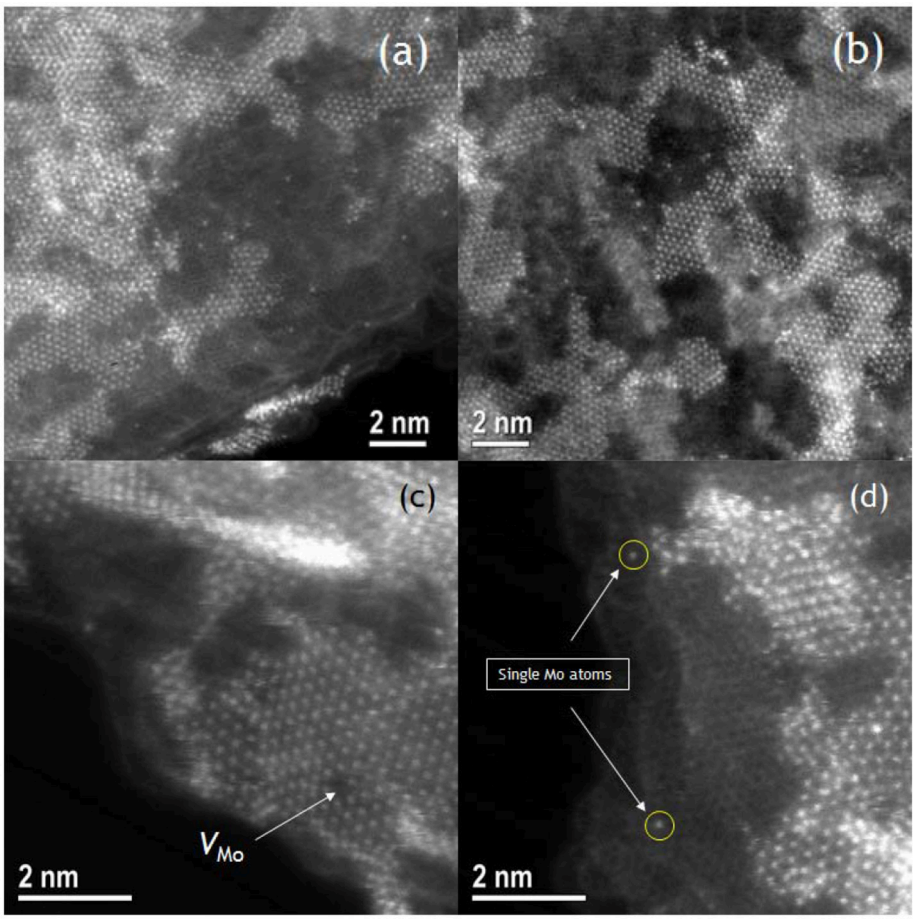

FIGURE 1 | Z-contrast STEM images of the MoS_2 flakes grown on few-layer r-GO.

the distribution of MoS_2 on the surface of the r-GO in the nanocomposite material.

The heterostructural nature of the MoS_2/r-GO nanocomposite was additionally identified by AFM. In **Figure 3**, we present the height and phase images (measured in tapping mode AFM) of MoS_2 nanosheets grown on few-layer r-GO. The AFM images of the MoS_2/r-GO nanocomposite deposited on a Si-wafer show the successful growth of MoS_2 layers on the graphene surface (**Figure 3**). The analysis of the height section profile (**Figure 4**) showed that the average thickness of the MoS_2 flakes on the r-GO sheets is around 4–8 nm, which corresponds to a few MoS_2 layers (∼5–10). Furthermore, the height profile analysis obtained at the edges of the r-GO sheets, showed a 1.5 nm thickness, a value typically reported for very few r-GO layers as also demonstrated from phase images.

XPS measurements were used in order to confirm the successful formation of MoS_2 on the r-GO surface. C1s (a), Mo3d (b), and S2p (c) XPS spectra of MoS_2/r-GO sample are shown in **Figure 5**. After deconvolution with mixed Gaussian–Lorentzian functions, the C1s spectrum consists of five components. The main peak at a binding energy of 284.6 eV, representing 53.1% of the total C1s area, is attributed to the C-C and C-H bonds. The component at 285.4 eV, contributing a 32.7% to the total C1s signal, is assigned to the hydroxyl C-O bonds as well as the C-N bonds from the oleyl amine. The third peak at 286.2 eV (9.0%) originates from the C-O-C epoxide/ether groups, whereas carbonyl functional groups (C=O) are associated with the peak at 287.3 eV (3.5%). Finally, the higher binding energy contribution recorded at 288.8 eV (1.7%) corresponds to the carboxyl groups (O-C=O) (Dimos et al., 2017; Kouloumpis et al., 2017; Tzitzios et al., 2017).

The domination of the C-C peak along with the high carbon content (80.8%) point out the presence of a r-GO substrate indicating the successful reduction of the starting GO. Due to the low concentration of the functionalizing oleyl amine and accordingly the even lower relative nitrogen atomic concentration, nitrogen and consequently oleyl amine were not detected by XPS. Nevertheless, its presence is verified by FTIR spectroscopy (see Figure S3), which is more effective for distinguishing organic molecules. The presence of oleyl amine in the r-GO and MoS_2/r-GO materials was indicated from the characteristic absorptions of the aliphatic and the amine groups in the IR spectra. The vibrations at 2,920 and 2,851 cm^{-1} are due to the symmetric and asymmetric stretching modes of CH_2, the weak band at 2962 arises from the asymmetric C-H stretching mode of the terminal CH_3 groups, while the double

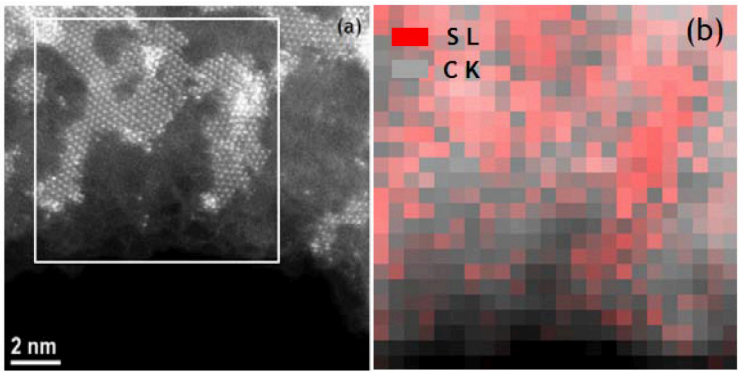

FIGURE 2 | Z-contrast STEM image **(a)** and EELS sulfur and carbon mapping **(b)** of MoS_2-decorated few layer r-GO. **(b)** corresponds to the white box area of **(a)**.

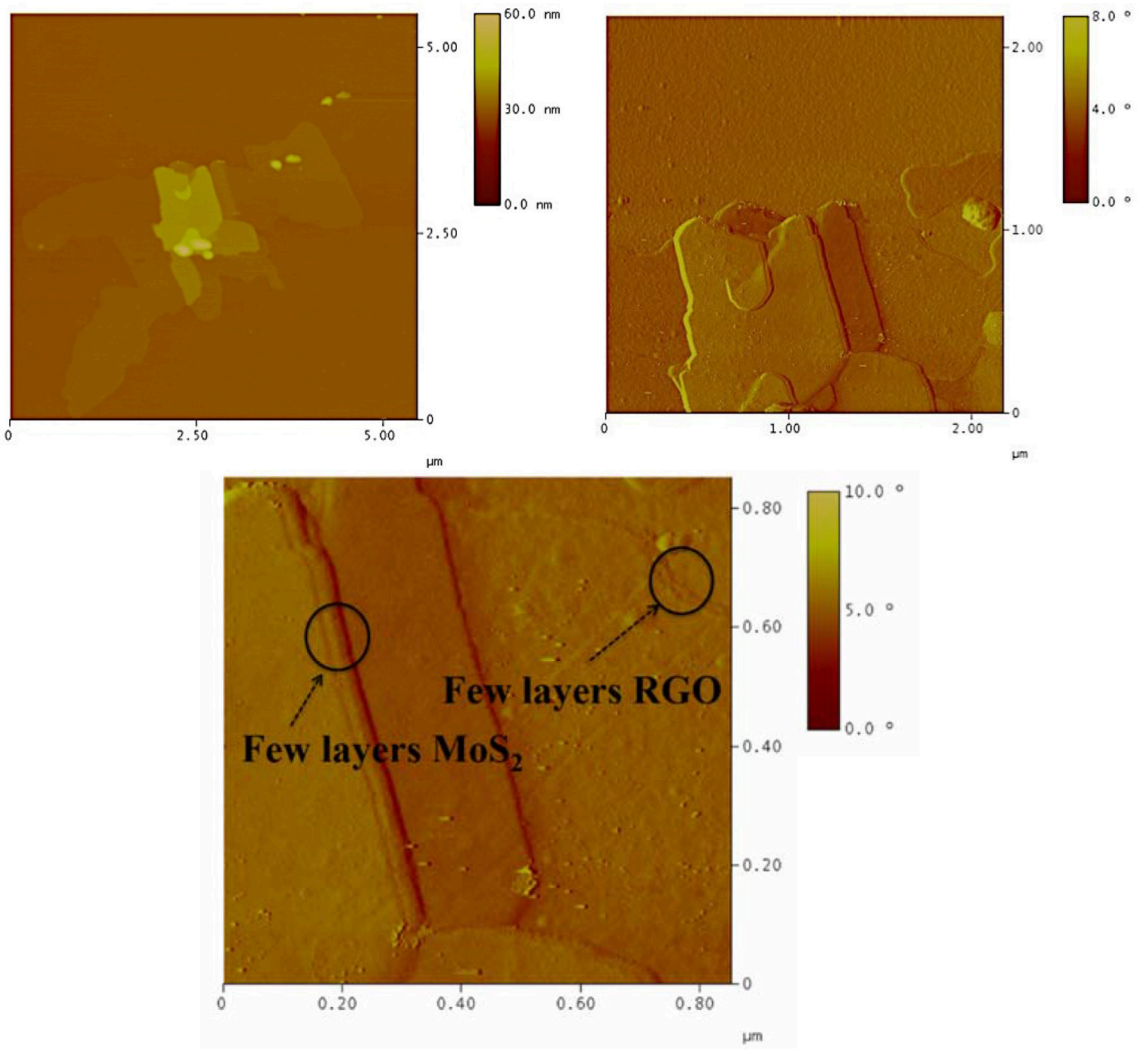

FIGURE 3 | AFM height **(left)** and phase (**right** and **bottom**) images of MoS_2/r-GO nanocomposite.

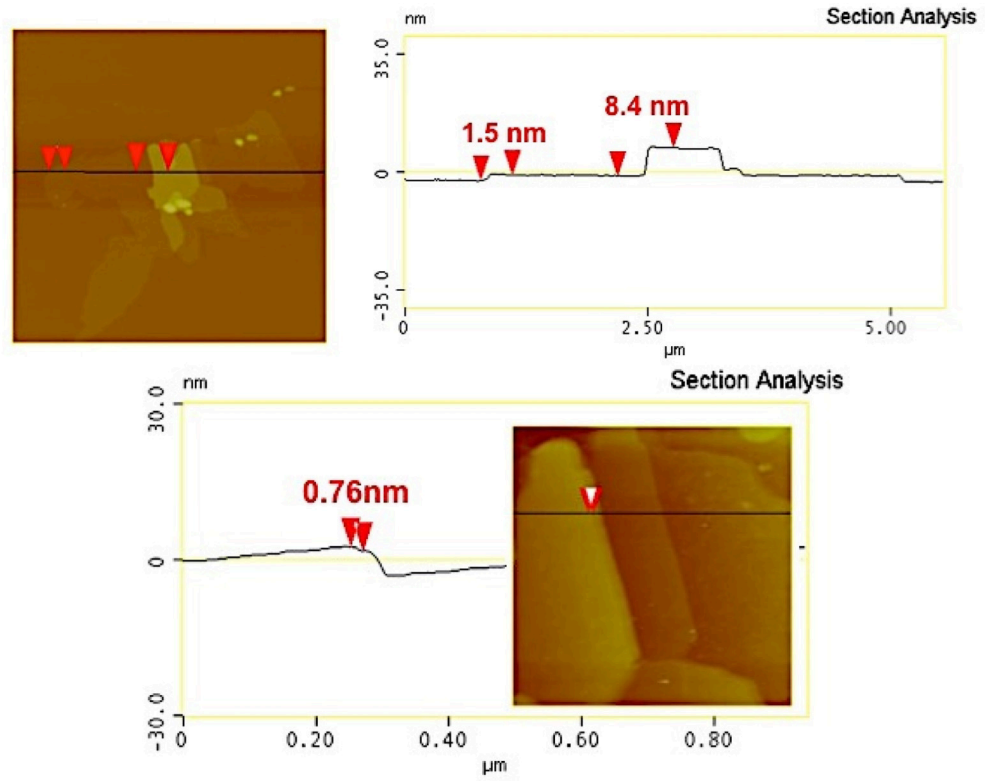

FIGURE 4 | AFM cross-section analysis of MoS_2/r-GO nanocomposite (a single MoS_2 layer can be distinguished from a package of few-layer MoS_2 sheets; picture below).

broad bands around 3,240–3,340 cm^{-1} arise from the stretching vibrations of the NH_2 group. The absence of these characteristic vibrations in the GO spectrum indirectly confirms the successful functionalization by the oleyl amine molecules. Furthermore, the absence of shifting of the N-H stretching band (around 3,300 cm^{-1} in pure oleyl amine), to lower wavenumbers indicates that the interaction of the NH_2 groups on the surface of both r-GO and MoS_2/r-GO is weak. On the other hand, molybdenum and sulfur were detected with an atomic concentration of 0.8 and 2.1% respectively proving the development of MoS_2 layers on the composite materials as simultaneously the S/Mo ratio is close to 2. In fact, from the distinction of the Mo and S species further conclusions can be deduced.

More specifically, as observed in **Figure 5b** of the Mo3d energy region, the spectrum consists of two Mo components. From their binding energies (229.4 and 232.4 eV), these peaks are ascribed as Mo^{IV} $3d_{5/2}$ and Mo^{IV} $3d_{3/2}$, respectively, and are correlated with MoS_2 structures (Spevack and McIntyre, 1993; Merki et al., 2011; Kibsgaard et al., 2012; Zheng et al., 2014). No peaks or shoulders are detected at higher binding energies, indicating the lack of higher oxidation states (+5 or +6) which are possible for Mo and suggesting the growth of further Mo_xS_y species except MoS_2 (Spevack and McIntyre, 1993; Merki et al., 2011; Kibsgaard et al., 2012; Zheng et al., 2014). Additionally, the peak at 227.0 eV is defined as S2s whilst more information about sulfur is obtained by the S2p XPS spectrum at **Figure 5c**. As in the case of Mo, only two peaks are observed; a main peak at 162.3 eV and a shoulder at 163.7 eV, associated with the doublet from S^{2-} $2p_{3/2}$ and S^{2-} $2p_{1/2}$ respectively (Spevack and McIntyre, 1993; Merki et al., 2011; Kibsgaard et al., 2012; Zheng et al., 2014). Again, no extra peaks are detected affirming that no S_2^{2-} or other species are present (Spevack and McIntyre, 1993; Merki et al., 2011; Kibsgaard et al., 2012; Zheng et al., 2014). In conclusion, the XPS study confirms the successful growth of MoS_2 structures on the composite material with a high content of 10.5 wt% (as deduced from the quantitative XPS analysis), excluding the creation of further Mo_xS_y species.

In addition, Raman spectroscopy is a powerful technique for both r-GO and MoS_2 materials, since it provides crucial information about the hybridization of atoms and the vibrational modes. As seen in the spectrum of the composite MoS_2/r-GO material (**Figure 6**), both r-GO-originating G- and D-bands are present as expected. The G-band at 1,594 cm^{-1} is associated with sp^2 hybridized carbon atoms, while the D-band at 1,345 cm^{-1} originates from the breathing modes of six-atom rings, requiring a defect for its activation, hence is correlated with lattice defects in the case of r-GO. Thus, the ratio of the D- to G-band intensities (I_D/I_G) states the defects ratio of the r-GO layers, (Tzitzios et al., 2017) and is equal to 0.86. A value slightly lower, as expected, than the one observed for starting GO (see Figure S4). Moreover,

peaks at the lower region of Raman shift are attributed to the formed MoS_2 layers. This region of the spectrum is multiplied 4 times compared to the rest spectrum in **Figure 6**, in order to have a clear view of the area. The peak at 407 cm^{-1} is assigned to the A_{1g} vibrational mode of MoS_2, while the one at 375 cm^{-1} originates from the corresponding E^1_{2g} mode (Lee et al., 2010; Kibsgaard et al., 2012; Sundaram et al., 2013; Zhang et al., 2013, 2015; David et al., 2014).

The distance between these two peaks has been correlated in the literature with the number of MoS_2 layers (Lee et al., 2010; Sundaram et al., 2013; Zhang et al., 2015). Unfortunately in our case, we cannot support the formation of single layers as

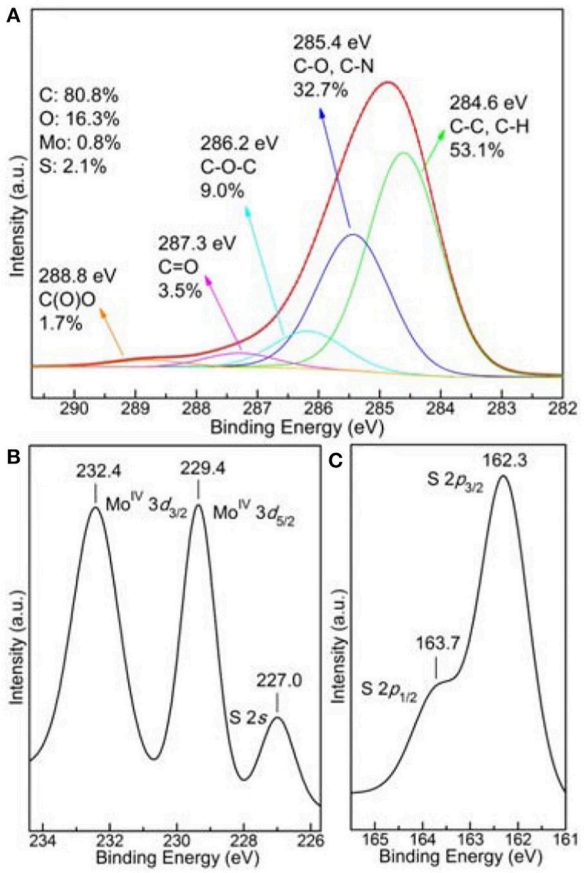

FIGURE 5 | C1s **(a)**, Mo3d **(b)**, and S2p **(c)**, X-ray photoemission spectra of MoS_2/r-GO nanocomposite.

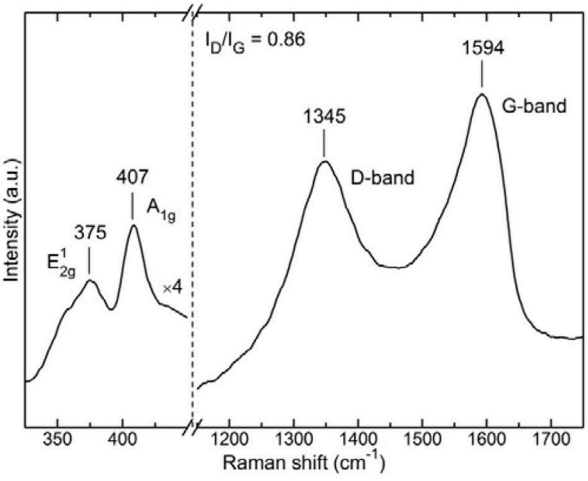

FIGURE 6 | Raman spectrum of the MoS_2/r-GO nanocomposite.

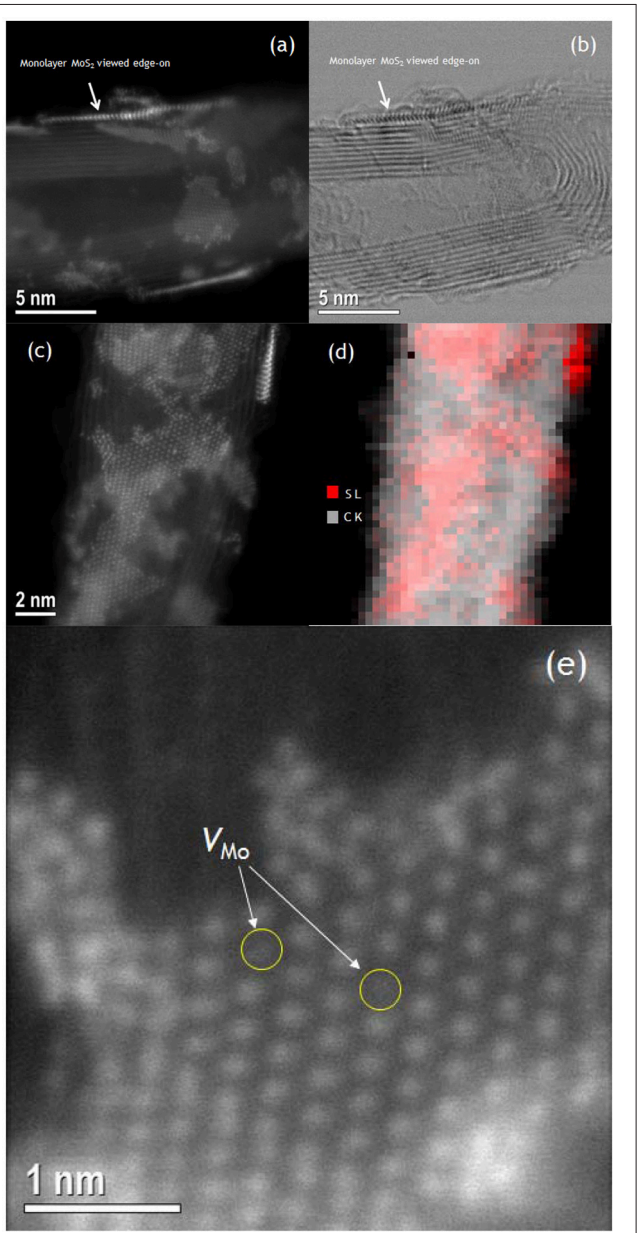

FIGURE 7 | Z-contrast STEM images **(a,c)**, bright field image **(b)** and EELS sulfur and carbon elemental mapping **(d)**, (with red and gray colors representing sulfur and carbon, respectively), of MoS_2/CN composites. Z-contrast image of monolayer MoS_2 on CN showing individual Mo vacancies **(e)**.

witnessed in TEM. This is because multilayers are also formed nearby and since the probing spot in Raman measurements was about 2 μm in diameter it was not possible to focus in a region with exclusively single layers of MoS_2. Nonetheless, the presence of both MoS_2 and r-GO peaks testify to the successful development of the composite material.

In order to study the generality of the methodology carbon nanotubes and carbon fibers were also used as support for the growth of MoS_2 layers. Both carbon nanotubes (CN), and carbon nanofibers (CNF), were first functionalized with oleyl amine followed by the growth of the MoS_2 using the same procedure. In **Figure 7**, we present STEM images of the MoS_2/CN composites. The images show similar behavior with the r-GO composites, i.e., the MoS_2 layers grow flat on the surface of the carbon nanotubes. It is worth mentioning here that, in the CN composites, most of the MoS_2 layers are single-layer, suggesting that the sp^2 nature of carbon is crucial for the uniform and single-layer growth of the MoS_2 on the surface of carbon-based materials. Atomic-resolution Z-contrast STEM images (**Figure 7e**) reveal the presence of Mo vacancies in the MoS_2 monolayers. The images of the corresponding composites with CNF are presented in the Supplementary Material section (Figure S5), and show clearly the uniform growth of mainly monolayer MoS_2 on the CNF surfaces.

In conclusion, in this work we report a facile liquid phase chemical approach for the synthesis of hybrid MoS_2/r-GO without autoclave conditions. The method is based on the thermolytic decomposition of $(NH_4)_2MoS_4$ inorganic salt in hot oleyl amine in the presence of chemically exfoliated r-GO. The r-GO sheets work as nucleation centers for the growth of MoS_2 and the composite material is composed mainly of single- to few-layer MoS_2 on few-layer r-GO. The use of oleyl amine functionalized r-GO as starting material for the growth of the MoS_2 seems to be crucial for the flat growth of MoS_2. In contrast, when GO is used as starting material, the MoS_2 layers do not grow flat. To our knowledge, it is the first time that MoS_2/r-GO is synthesized in non-polar media without autoclave conditions and the final hybrid nanocomposites are well dispersible in non-polar solvents such as n-hexane. The methodology is generally applicable and works in a similar way in the case of MoS_2 growth on the surface of other carbon-based materials such as multiwall carbon nanotubes (CN) and carbon nanofibers (CNF). This kind of colloidal dispersion can be applicable in the formation of films through inkjet printing techniques (Arapov et al., 2014).

AUTHOR CONTRIBUTIONS

VT developed the synthesis concept, synthesized the materials and with SA, and GP prepared the manuscript; KD contributed to the manuscript preparation, and with AK, DG, and MAK performed the AFM, XPS and Raman spectroscopy studies; GB, YA, HJ, MK, and MF carried out the structural and the surface functionalization studies; RM, MR, NB, J-CI, SJP, AB, and STP carried out the STEM studies. All authors discussed the results and commented on the manuscript.

ACKNOWLEDGMENTS

This work is partially funded by the Petroleum Institute (a part of Khalifa University of Science and Technology). Electron microscopy work at Oak Ridge National Laboratory (ORNL) was supported by the U.S. Department of Energy (DOE) Office of Science, Basic Energy Sciences (BES), Materials Science and Engineering Directorate (MR) and through a user project conducted at the Center for Nanophase Materials Sciences, which is a DOE Office of Science User Facility (J-CI, RM).Work at Vanderbilt University was supported by the U. S. Department of Energy grant DE-FG02-09ER-46554 (RM, STP) and the McMinn Endowment.

SUPPLEMENTARY MATERIAL

The Supplementary Material for this article can be found online at: https://www.frontiersin.org/articles/10.3389/fmats.2018.00029/full#supplementary-material

REFERENCES

Arapov, K., Abbel, R., de With, G., and Friedrich, H. (2014). Inkjet printing of graphene. *Faraday Discuss*. 173, 323–336. doi: 10.1039/C4FD00067F

Chang, K., and Chen, W. (2011). Single-layer MoS_2/graphene dispersed in amorphous carbon: towards high electrochemical performances in rechargeable lithium ion batteries. *J. Mater. Chem.* 21:17175. doi: 10.1039/c1jm12942b

Chen, J., Tang, W., Tian, B., Liu, B., Zhao, X., Liu, Y., et al. (2016). Chemical vapor deposition of high-quality large-sized MoS_2 crystals on silicon dioxide substrates. *Adv. Sci.* 3:1500033. doi: 10.1002/advs.201600033

Coleman, J. N., Lotya, M., O'Neill, A., Bergin, S. D., King, P. J., Khan, U., et al. (2011). Two-dimensional nanosheets produced by liquid exfoliation of layered materials. *Science* 331, 568–571. doi: 10.1126/science.1194975

Conley, H. J., Wang, B., Ziegler, J. I., Haglund, R. F., Pantelides, S. T., and Bolotin, K. I. (2013). Bandgap engineering of strained monolayer and bilayer MoS_2. *Nano Lett.* 13, 3626–3630. doi: 10.1021/nl4014748

David, L., Bhandavat, R., and Singh, G. (2014). MoS_2/graphene composite paper for sodium-ion battery electrodes. *ACS Nano* 8, 1759–1770. doi: 10.1021/nn406156b

Dean, C. R., Young, A. F., Meric, I., Lee, C., Wang, L., Sorgenfrei, S., et al. (2010). Boron nitride substrates for high-quality graphene electronics. *Nat. Nanotechnol.* 5, 722–726. doi: 10.1038/nnano.2010.172

Dimos, K., Arcudi, F., Kouloumpis, A., Koutselas, I. B., Rudolf, P., Gournis, D., et al. (2017). Top-down and bottom-up approaches to transparent, flexible and luminescent nitrogen-doped carbon nanodot-clay hybrid films. *Nanoscale* 9, 10256–10262. doi: 10.1039/C7NR02673K

Geim, A. K., and Novoselov, K. S. (2007). The rise of graphene. *Nat. Mater.* 6, 183–191. doi: 10.1038/nmat1849

Gengler, R. Y., Veligura, A., Enotiadis, A., Diamanti, E. K., Gournis, D., Józsa, C., et al. (2010). Large-yield preparation of high-electronic-quality graphene by a langmuir–schaefer approach. *Small* 6, 35–39. doi: 10.1002/smll.200901120

Jaramillo, T. F., Jorgensen, K. P., Bonde, J., Nielsen, J. H., Horch, S., and Chorkendorff, I. (2007). Identification of active edge sites for electrochemical H2 evolution from MoS_2 nanocatalysts. *Science* 317, 100–102. doi: 10.1126/science.1141483

Kibsgaard, J., Chen, Z., Reinecke, B. N., and Jaramillo, T. F. (2012). Engineering the surface structure of MoS_2 to preferentially expose active edge sites for electrocatalysis. *Nat. Mater.* 11, 963–969. doi: 10.1038/nmat3439

Kong, D., Wang, H., Cha, J. J., Pasta, M., Koski, K. J., Yao, J., et al. (2013). Synthesis of MoS_2 and $MoSe_2$ films with vertically aligned layers. *Nano Lett.* 13, 1341–1347. doi: 10.1021/nl400258t

Koroteev, V. O., Bulusheva, L. G., Okotrub, A. V., Yudanov, N. F., and Vyalikh, D. V. (2011). Formation of MoS_2 nanoparticles on the surface of reduced graphite oxide. *Phys. Status Solidi* 248, 2740–2743. doi: 10.1002/pssb.201100123

Kouloumpis, A., Thomou, E., Chalmpes, N., Dimos, K., Spyrou, K., Bourlinos, A. B., et al. (2017). Graphene/carbon dot hybrid thin films prepared by a modified langmuir–schaefer method. *ACS Omega* 2, 2090–2099. doi: 10.1021/acsomega.7b00107

Lee, C., Yan, H., Brus, L. E., Heinz, T. F., Hone, J., and Ryu, S. (2010). Anomalous lattice vibrations of single- and few-layer MoS_2. *ACS Nano* 4, 2695–2700. doi: 10.1021/nn1003937

Lembke, D., and Kis, A. (2012). Breakdown of high-performance monolayer MoS_2 transistors. *ACS Nano* 6, 10070–10075. doi: 10.1021/nn303772b

Li, Y., Wang, H., Xie, L., Liang, Y., Hong, G., and Dai, H. (2011). MoS_2 Nanoparticles grown on graphene: an advanced catalyst for the hydrogen evolution reaction. *J. Am. Chem. Soc.* 133, 7296–7299. doi: 10.1021/ja201269b

Liao, L., Zhu, J., Bian, X., Zhu, J., Scanlon, M. D., Girault, H. H., et al. (2013). MoS_2 formed on mesoporous graphene as a highly active catalyst for hydrogen evolution. *Adv. Funct. Mater.* 23, 5326–5333. doi: 10.1002/adfm.201300318

Ma, L., Huang, G., Chen, W., Wang, Z., Ye, J., Li, H., et al. (2014). Cationic surfactant-assisted hydrothermal synthesis of few-layer molybdenum disulfide/graphene composites: microstructure and electrochemical lithium storage. *J. Power Sources* 264, 262–271. doi: 10.1016/j.jpowsour.2014.04.084

Ma, Y., Dai, Y., Guo, M., Niu, C., and Huang, B. (2011). Graphene adhesion on MoS_2 monolayer: an ab initio study. *Nanoscale* 3, 3883–3887. doi: 10.1039/c1nr10577a

Merki, D., Fierro, S., Vrubel, H., and Hu, X. (2011). Amorphous molybdenum sulfide films as catalysts for electrochemical hydrogen production in water. *Chem. Sci.* 2, 1262–1267. doi: 10.1039/C1SC00117E

Radisavljevic, B., Radenovic, A., Brivio, J., Giacometti, V., and Kis, A. (2011). Single-layer MoS_2 transistors. *Nat. Nanotechnol.* 6, 147–150. doi: 10.1038/nnano.2010.279

Samad, L., Bladow, S. M., Ding, Q., Zhuo, J., Jacobberger, R. M., Arnold, M. S., et al. (2016). Layer-controlled chemical vapor deposition growth of MoS_2 vertical heterostructures via van der waals epitaxy. *ACS Nano* 10, 7039–7046. doi: 10.1021/acsnano.6b03112

Shi, Y., Zhou, W., Lu, A.-Y., Fang, W., Lee, Y.-H., Hsu, A. L., et al. (2012). van der Waals epitaxy of MoS_2 layers using graphene as growth templates. *Nano Lett.* 12, 2784–2791. doi: 10.1021/nl204562j

Spevack, P. A., and McIntyre, N. S. (1993). A Raman and XPS investigation of supported molybdenum oxide thin films. 2. Reactions with hydrogen sulfide. *J. Phys. Chem.* 97, 11031–11036. doi: 10.1021/j100144a021

Staudenmaier, L. (1898). Verfahren zur Darstellung der Graphitsäure. *Berichte der Deutschen Chemischen Gesellschaft* 31, 1481–1487. doi: 10.1002/cber.18980310237

Stergiou, D. V., Diamanti, E. K., Gournis, D., and Prodromidis, M. I. (2010). Comparative study of different types of graphenes as electrocatalysts for ascorbic acid. *Electrochem. Commun.* 12, 1307–1309. doi: 10.1016/j.elecom.2010.07.006

Sundaram, R. S., Engel, M., Lombardo, A., Krupke, R., Ferrari, A. C., Avouris, P., et al. (2013). Electroluminescence in Single Layer MoS_2. *Nano Lett.* 13, 1416–1421. doi: 10.1021/nl400516a

Tzitzios, V., Hu, X., Dimos, K., Gournis, D., Georgakilas, V., Avgouropoulos, G., et al. (2017). Uniform growth of fct FePt nanoparticles on the surface of reduced-GO via a green facile approach. Ferromagnetic r-GO nanocomposites with high coercivity and surface area. *Carbon* 121, 209–216. doi: 10.1016/j.carbon.2017.05.077

Wang, H., Lu, Z., Kong, D., Sun, J., Hymel, T. M., and Cui, Y. (2014). Electrochemical tuning of MoS_2 nanoparticles on three-dimensional substrate for efficient hydrogen evolution. *ACS Nano* 8, 4940–4947. doi: 10.1021/nn500959v

Wang, H., Yu, L., Lee, Y.-H., Shi, Y., Hsu, A., Chin, M., et al. (2012). Integrated circuits based on bilayer MoS_2 transistors. *Nano Lett.* 12, 4674–4680. doi: 10.1021/nl302015v

Xiang, Q., Yu, J., and Jaroniec, M. (2012). Synergetic effect of MoS_2 and graphene as cocatalysts for enhanced photocatalytic H_2 production activity of TiO_2 nanoparticles. *J. Am. Chem. Soc.* 134, 6575–6578. doi: 10.1021/ja302846n

Zhang, W., Chuu, C. P., Huang, J. K., Chen, C. H., Tsai, M. L., Chang, Y. H., et al (2015). Ultrahigh-gain photodetectors based on atomically thin graphene-MoS_2 heterostructures. *Sci. Rep.* 4:3826. doi: 10.1038/srep03826

Zhang, X., Han, W. P., Wu, J. B., Milana, S., Lu, Y., Li, Q. Q., et al. (2013). Raman spectroscopy of shear and layer breathing modes in multilayer MoS_2 *Phys. Rev. B* 87, 1154131–1154138. doi: 10.1103/PhysRevB.87.115413

Zheng, X., Xu, J., Yan, K., Wang, H., Wang, Z., and Yang, S. (2014). Space-confined growth of MoS_2 nanosheets within graphite: the layered hybrid of MoS_2 and graphene as an active catalyst for hydrogen evolution reaction. *Chem. Mater.* 26, 2344–2353. doi: 10.1021/cm500347r

Zobel, A., Boson, A., Wilson, P. M., Muratov, D. S., Kuznetsov, D. V., and Sinitskii, A. (2016). Chemical vapour deposition and characterization of uniform bilayer and trilayer MoS_2 crystals. *J. Mater. Chem. C* 4, 11081–11087. doi: 10.1039/C6TC03587F

Conflict of Interest Statement: The authors declare that the research was conducted in the absence of any commercial or financial relationships that could be construed as a potential conflict of interest.